# High-Efficiency Voltage-Clamped DC–DC Converter With Reduced Reverse-Recovery Current and Switch-Voltage Stress

Rong-Jong Wai, *Senior Member, IEEE*, Li-Wei Liu, and Rou-Yong Duan

***Abstract*—This paper investigates a high-efficiency clamped-voltage dc–dc converter with reduced reverse-recovery current and switch-voltage stress. In the circuit topology, it is designed by way of the combination of inductor and transformer to increase the corresponding voltage gain. Moreover, one additional inductor provides the reverse-current path of the transformer to enhance the utility rate of magnetic core. In addition, the voltage-clamped technology is used to reduce the switch-voltage stress so that it can select the Schottky diode in the output terminal for alleviating the reverse-recovery current and decreasing the switching and conduction losses. Furthermore, the closed-loop control methodology is utilized in the proposed scheme to overcome the voltage-drift problem of power source under the variation of loads. Thus, the proposed converter topology has a favorable voltage-clamped effect and superior conversion efficiency. Some experimental results via an example of a proton-exchange-membrane fuel cell (PEMFC) power source with a 250-W nominal rating are given to demonstrate the effectiveness of the proposed power-conversion strategy.**

***Index Terms*—Converter, fuel cell, proton-exchange membrane (PEM), reverse recovery, voltage clamped.**

## I. Introduction

In RECENT years, dc–dc converters with steep voltage ratio are usually required in many industrial applications, e.g., the front-end stage for clean energy sources, the dc backup energy system for an uninterruptible power supply (UPS), high-intensity discharge (HID) lamps for automobile headlamps, and the telecommunication industry [1]–[3]. The conventional boost converters cannot provide such a high dc-voltage ratio due to the losses associated with the inductor, filter capacitor, main switch, and output diode. Even for an extreme duty cycle, it will result in serious reverse-recovery problems and increase the rating of the output diode. As a result, the conversion efficiency is degraded, and the electromagnetic interference (EMI) problem is severe under this situation [4]. In order to increase the conversion efficiency and voltage gain, many modified boost-converter topologies have been investigated in the past decade [5]–[10].

Although voltage-clamped techniques are manipulated in the converter design to overcome the severe reverse-recovery problem of the output diode in high-level voltage applications, there still exist overlarge switch-voltage stresses, and the voltage gain is limited by the turn-ON time of the auxiliary switch [5], [6]. da Silva *et al.* [7] presented a boost soft-single-switch converter, which has only one single active switch. It is able to operate with soft switching in a pulsewidth modulation (PWM) way without high voltage and current stresses. Unfortunately, the voltage gain is limited below four in order to achieve the function of soft switching. In [8] and [9], coupled inductors were employed to provide a high step-up ratio and to reduce the switch-voltage stress substantially, and the reverse-recovery problem of the output diode was also alleviated efficiently. In this case, the leakage energy of the coupled inductor is another problem as the main switch was turned OFF. It will result in a high-voltage ripple across the main switch due to the resonant phenomenon induced by the leakage current. In order to protect the switch devices, either a high-voltage-rated device with higher $R_{\mathrm{DS(ON)}}$ or a snubber circuit is usually adopted to deplete the leakage energy. Consequently, the power-conversion efficiency will be degraded. Zhao and Lee [10] introduced a family of high-efficiency high-step-up dc–dc converters by only adding one addition diode and a small capacitor. It can recycle the leakage energy and alleviate the reverse-recovery problem. However, a snubber circuit is still required in the output diode terminal with extra energy losses.

Nowadays, fuel cells are in the news because they appear to be one of the most efficient and effective solutions to the environmental pollution problem [11]–[17]. A fuel cell is an energy conversion device that produces electricity by electrochemically combining fuel (hydrogen) and oxidant (oxygen from the air) gases through electrodes, across an ion conduction electrolyte. This process produces much higher conversion efficiency than any conventional thermal-mechanical system, because it operates without combustion and extracts more electricity from the same amount of fuel. This system has the merits of high efficiency, energy security, reliability, pollution free, and quiet operations. Fuel cells have been known to science for more than 160 years and have recently become the subject of intense research and development. Up to the present, many demonstration projects have shown fuel-cell

Manuscript received May 19, 2004; revised July 19, 2005. Abstract published on the Internet November 25, 2005. This work was supported by the National Science Council of Taiwan, R.O.C., under Grant NSC 92-2623-7-155-014, and by the Ministry of Economic Affairs of Taiwan, R.O.C., under Grant 92-EC-17-A-05-S1-0012.

R.-J. Wai is with the Department of Electrical Engineering, Yuan Ze University, Chung Li, Taiwan, R.O.C. (e-mail: rjwai@saturn.yzu.edu.tw).

L.-W. Liu was with the Department of Electrical Engineering, Yuan Ze University, Chung Li, Taiwan, R.O.C. He is now with the Department of Test and Measurement, Chroma Company, Taipei, Taiwan, R.O.C.

R.-Y. Duan is with the Department of Industrial Safety and Health, Hung Kuang University, Tai Chung, Taiwan, R.O.C.

Digital Object Identifier 10.1109/TIE.2005.862251

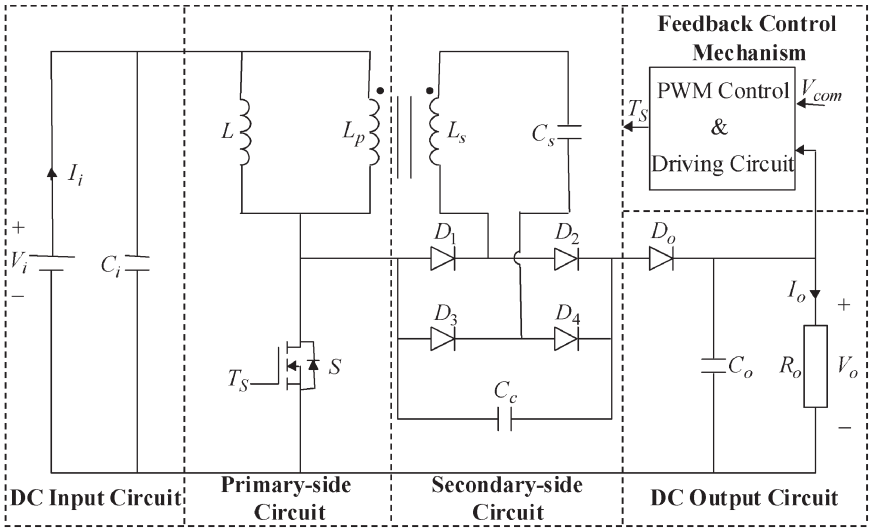


Fig. 1. System configuration of a high-efficiency voltage-clamped dc–dc converter.

systems to be feasible for portable power, transportation, utility power and on-site power generation in a variety of building applications.

For portable power, a fuel cell with a fuel container can offer a higher-energy density and more convenience than conventional battery systems. Moreover, portable power packs using fuel cells can be lighter and smaller in volume for an equivalent amount of energy. In transportation applications, fuel cells offer higher efficiency and better part-load performance than conventional engines. In stationary power applications, low emissions permit fuel cells to be located in high-power requirement areas, where they can supplement the existing utility grid. Using fuel cells and hydrogen technology, electrical power can be delivered cleanly, efficiently and sustainability where and when required. The greatest research interests throughout the world have focussed on proton-exchange membrane (PEM) and solid oxide cell stacks. Specially, PEM fuel cell (PEMFC) has promising characteristics as follows: 1) the by-product waste is water; 2) low-temperature operation; and 3) they use a solid polymer as the electrolyte that reduces concerns related to construction, transportation, and safety issues [16]. Thus, it seems to be a good alternative source for distributed generation systems.

The aim of this study is to design a high-efficiency voltage-clamped dc–dc converter with reduced reverse-recovery current and switch-voltage stress to provide a stable constant dc voltage. To achieve this goal, the manipulation of inductor and transformer is adopted to increase the voltage gain and to enhance the utility rate of the magnetic core. Moreover, the voltage-clamped technology is used for reducing the switch-voltage stress and solving the reverse-recovery problem. In addition, the closed-loop control methodology is utilized in the proposed converter to overcome the voltage-drift problem of power source under the variation of loads. The prototype is developed for a PEMFC application requiring an output power of 310 W, an output voltage of 200 V, and an input voltage varying from 27 to 37.5 V. The remainder of this study is organized as follows. Section II presents the converter design and analyses in detail. Experimental results for a PEMFC power source with a 250-W nominal rating are provided to validate the effectiveness of the proposed power-conversion system in Section III. Conclusions are drawn in Section IV.

## II. Converter Design and Analyses

A newly designed converter topology is depicted in Fig. 1, where it contains five parts including a dc-input circuit, a primary-side circuit, a secondary-side circuit, a dc-output circuit, and a feedback-control mechanism. The major symbol representations are summarized as follows. $V_{\rm i}$ and $I_{\rm i}$ denote the dc-input voltage and current, and $C_{\rm i}$ is the input filter capacitor in the dc-input circuit. $L_{\rm p}$ represents the primary inductor of the transformer; $L$ is the additional inductor in the primary-side circuit; and $S$ is the main switch. $L_{\rm s}$ denotes the secondary inductor of the transformer; $C_{\rm s}$ and $C_{\rm c}$ are the balanced capacitor and clamped capacitor in the secondary-side circuit; and $D_1$, $D_2$, $D_3$, and $D_4$ are the rectifier diodes. $V_{\rm o}$ and $I_{\rm o}$ describe the output voltage and current; $R_{\rm o}$ is the output load; $D_{\rm o}$, and $C_{\rm o}$ are the output diode and filter capacitor in the output circuit. $V_{\rm com}$ and $T_{\rm S}$ are the output-voltage command and switch-driving signal in the feedback-control mechanism, respectively.

The equivalent circuit and state definition of the newly designed converter is depicted in Fig. 2, where the transformer is modeled as an ideal transformer with a secondary leakage inductor $(L_{\rm k})$. The turns ratio of this ideal transformer is defined as

$$n = \frac{N_2}{N_1} \tag{1}$$

where $N_1$ and $N_2$ are the primary and secondary winding turns. The additional inductor $(L)$ is located in parallel with the primary side of the transformer. Moreover, the rectifier diodes ($D_1$, $D_2$, $D_3$, and $D_4$) are connected between the primary and secondary sides of the transformer. The voltages across the additional inductor, the main switch, the ideal transformer primary

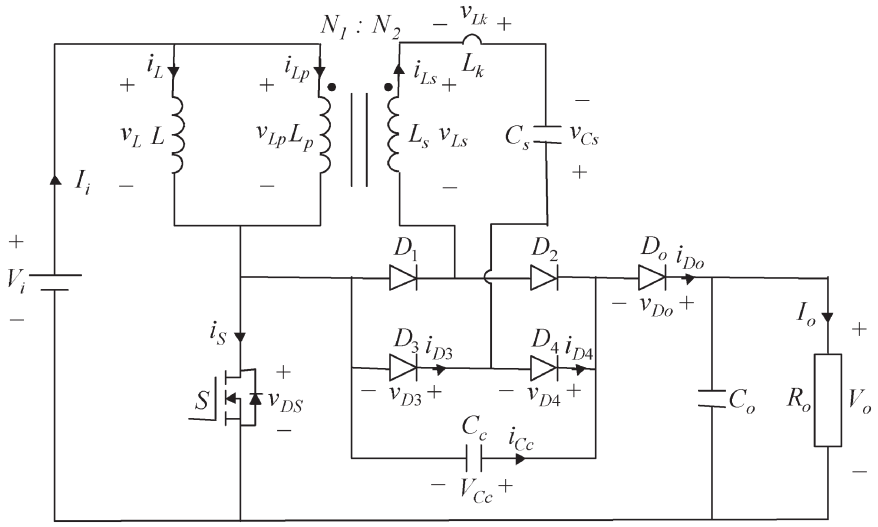


Fig. 2. Equivalent circuit.

and secondary winding, the secondary leakage inductor, the balanced capacitor, and the output diode are $v_L$, $v_{\rm DS}$, $v_{L_{\rm p}}$, $v_{L_{\rm s}}$, $v_{L_{\rm k}}$, $v_{C_{\rm s}}$, and $v_{\rm Do}$, respectively. The clamped capacitor $C_{\rm c}$ is assumed to be large enough to be viewed as a constant voltage source, $V_{C_{\rm c}}$. The conductive voltage drops of the main switch $(S)$ and all diodes ($D_1$, $D_2$, $D_3$, $D_4$, and $D_{\rm o}$) are neglected to simplify the circuit analyses. The characteristic waveforms of the proposed high-efficiency converter are depicted in Fig. 3. In addition, Fig. 4 illustrates the operational modes in one switching cycle, and the detailed operation stages are described as follows.

### A. Mode 1 $(t_0 - t_1)$ [Fig. 4(a)]

At time $t = t_0$, the main switch $(S)$ is turned ON. At the same time, the diodes ($D_1$ and $D_4$) become conducted, and other diodes ($D_2$, $D_3$, and $D_{\rm o}$) are reverse biased. The additional inductor $(L)$ and clamped capacitor $(C_{\rm c})$ are linearly charged by the input-voltage source $(V_{\rm i})$ through the transformer. Applying Kirchhoff's law [4], the voltages of $v_L$, $v_{L_{\rm p}}$, $v_{L_{\rm s}}$, and $v_{L_{\rm k}}$ during this period can be expressed as

$$v_L = v_{L_{\rm p}} = V_{\rm i} \tag{2}$$

$$v_{L_{\rm s}} = nV_{\rm i} \tag{3}$$

$$v_{L_{\rm k}} = V_{C_{\rm c}} - nV_{\rm i} - v_{C_{\rm s}}. \tag{4}$$

According to (2)–(4), the rate of change of the additional inductor current $(i_L)$, the primary-side current $(i_{L_{\rm p}})$, and the secondary-side current $(i_{L_{\rm s}})$ of the transformer can be represented as

$$\frac{di_L}{dt} = \frac{V_{\rm i}}{L} \tag{5}$$

$$\frac{di_{L_{\rm p}}}{dt} = \frac{V_{C_{\rm c}} - nV_{\rm i} - v_{C_{\rm s}}}{L_{\rm k}} + \frac{V_{\rm i}}{L_{\rm p}} \tag{6}$$

$$\frac{di_{L_{\rm s}}}{dt} = \frac{V_{C_{\rm c}} - nV_{\rm i} - v_{C_{\rm s}}}{L_{\rm k}}. \tag{7}$$

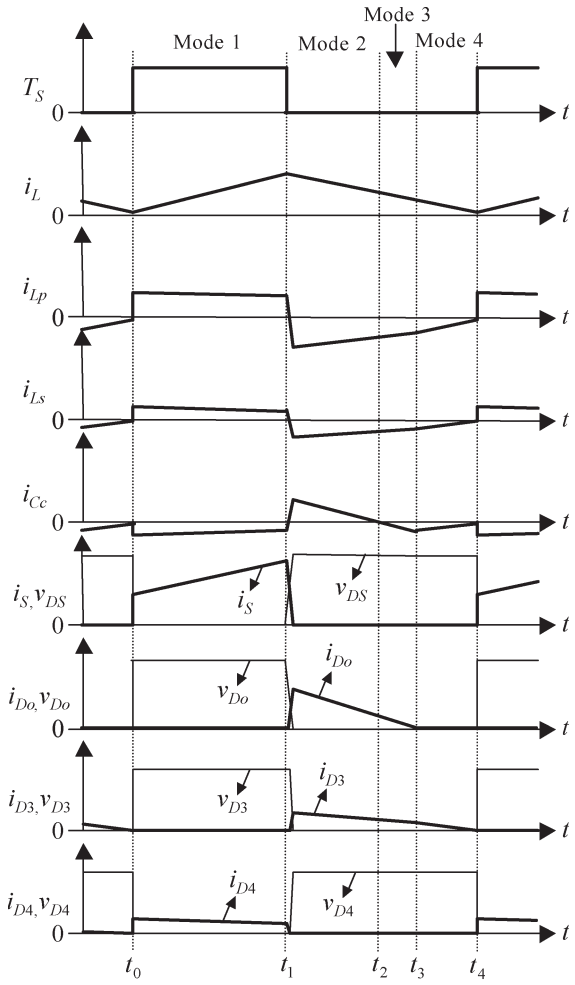


Fig. 3. Characteristic waveforms.

### B. Mode 2 $(t_1 - t_2)$ [Fig. 4(b)]

At time $t = t_1$, the main switch $(S)$ is turned OFF. At this time, the diodes ($D_2$, $D_3$, and $D_{\rm o}$) become forward biased to start conducting, and other diodes ($D_1$ and $D_4$) are reverse biased. The stored energy of the additional inductor $(L)$ and

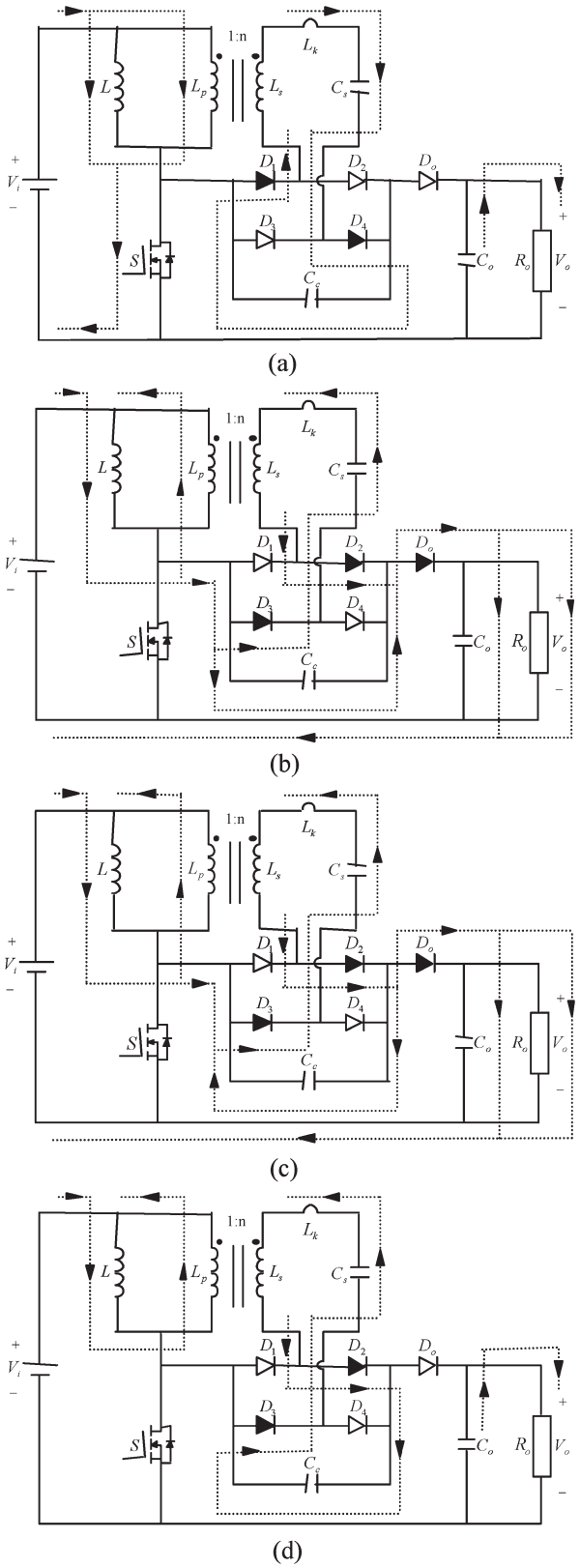


Fig. 4. Operational modes: (a) mode 1 $[t_0 - t_1]$; (b) mode 2 $[t_1 - t_2]$; (c) mode 3 $[t_2 - t_3]$; (d) mode 4 $[t_3 - t_4]$.

clamped capacitor $(C_{\rm c})$ in Mode 1 is released to output loads. Moreover, the transformer can be operated at four quadrants to enhance the utility rate of the magnetic core and to keep the clamped voltage $(V_{C_{\rm c}})$, since the additional inductor $(L)$ supplies energy to the output terminal by way of the transformer. Applying Kirchhoff's law [4], the voltage and current relations of each element during this mode can be described by

$$v_L = v_{L_{\rm p}} = V_{\rm i} + V_{C_{\rm c}} - V_{\rm o} \tag{8}$$

$$v_{L_{\rm s}} = n(V_{\rm i} + V_{C_{\rm c}} - V_{\rm o}) \tag{9}$$

$$v_{L_{\rm k}} = -V_{C_{\rm c}} - v_{C_{\rm s}} - n(V_{\rm i} + V_{C_{\rm c}} - V_{\rm o}) \tag{10}$$

$$v_{\rm DS} = V_{\rm i} - V_L = V_{\rm o} - V_{C_{\rm c}} < V_{\rm o} \tag{11}$$

$$i_{D_{\rm o}} = i_L + i_{L_{\rm p}} = i_{C_{\rm c}} - i_{L_{\rm s}} \tag{12}$$

where $i_{D_{\rm o}}$ is the current of the output diode $D_{\rm o}$; $i_{C_{\rm c}}$ is the current of the clamped capacitor $C_{\rm c}$. According to (11), the cutoff voltage of the main switch $(S)$ is clamped at $V_{\rm o} - V_{C_{\rm c}}$. Moreover, the main switch $(S)$ with low-voltage-rated capacity can be selected since the switch-voltage stress $(v_{\rm DS})$ is smaller than the output voltage $(V_{\rm o})$. The selection of a low-voltage-rated device with lower $R_{\rm DS(ON)}$ is useful for improving the conversion efficiency. Referring to (8)–(10), the rate of change of $i_L$, $i_{L_{\rm p}}$ and $i_{L_{\rm s}}$ is given by

$$\frac{di_L}{dt} = \frac{V_{\rm i} + V_{C_{\rm c}} - V_{\rm o}}{L} \tag{13}$$

$$\frac{di_{L_{\rm p}}}{dt} = \frac{-V_{C_{\rm c}} - v_{C_{\rm s}} - n(V_{\rm i} + V_{C_{\rm c}} - V_{\rm o})}{L_{\rm k}} + \frac{V_{\rm i} + V_{C_{\rm c}} - V_{\rm o}}{L_{\rm p}} \tag{14}$$

$$\frac{di_{L_{\rm s}}}{dt} = \frac{-V_{C_{\rm c}} - v_{C_{\rm s}} - n(V_{\rm i} + V_{C_{\rm c}} - V_{\rm o})}{L_{\rm k}}. \tag{15}$$

### C. Mode 3 $(t_2 - t_3)$ [Fig. 4(c)]

At time $t = t_2$, the residual energy of the clamped capacitor $(C_{\rm c})$ is discharged entirely, i.e., $i_{C_{\rm c}}(t_2) = 0$. Immediately, the clamped capacitor $(C_{\rm c})$ is charged by the energy of the additional inductor $(L)$ through the transformer, and the rate of change of the clamped-capacitor current $(i_{C_{\rm c}})$ can be denoted as

$$\frac{di_{C_{\rm c}}}{dt} = \frac{V_{\rm i} + V_{C_{\rm c}} - V_{\rm o}}{L} + \frac{V_{\rm i} + V_{C_{\rm c}} - V_{\rm o}}{L_{\rm p}} + 2\left[\frac{-V_{C_{\rm c}} - v_{C_{\rm s}} - n(V_{\rm i} + V_{C_{\rm c}} - V_{\rm o})}{L_{\rm k}}\right]. \tag{16}$$

Moreover, the stored energy of the additional inductor $(L)$ is released continuously to the output terminal by way of the transformer. The rate of charge of $i_{D_{\rm o}}$ is given by

$$\frac{di_{D_{\rm o}}}{dt} = \frac{V_{\rm i} + V_{C_{\rm c}} - V_{\rm o}}{L} + \frac{V_{\rm i} + V_{C_{\rm c}} - V_{\rm o}}{L_{\rm p}} + \frac{-V_{C_{\rm c}} - v_{C_{\rm s}} - n(V_{\rm i} + V_{C_{\rm c}} - V_{\rm o})}{L_{\rm k}}. \tag{17}$$

### D. Mode 4 $(t_3 - t_4)$ [Fig. 4(d)]

At time $t = t_3$, the clamped-capacitor current $(i_{C_{\rm c}})$ equals to the secondary-side current $(i_{L_{\rm s}})$ of the transformer, and

the output diode current ($i_{D_o}$) decays to 0, i.e., $i_{D_o}(t_3) = 0$. During this period, the voltage of the output diode ($v_{D_o}$) maintains the zero status until the main switch ($S$) is turned ON. Moreover, the magnitude of the additional inductor current ($i_L$) is equal to the one of the primary-side current ($i_{L_p}$). According to (13) and (14), the rate of change of $i_{L_p}$ and $i_{L_s}$ can be represented as

$$\frac{di_{L_p}}{dt} = -\frac{di_L}{dt} = -\frac{V_i + V_{C_c} - V_o}{L} \tag{18}$$

$$\frac{di_{L_s}}{dt} = -\frac{V_i + V_{C_c} - V_o}{L} - \frac{V_i + V_{C_c} - V_o}{L_p}. \tag{19}$$

Since the secondary leakage inductor ($L_k$) and the change rate of $i_{L_s}$ in the transformer are very small, the voltage of the secondary leakage inductor ($v_{L_k}$) can be neglected. According to the concept of the zero average voltage across the inductor over one period [4], the voltages of $v_{C_s}$, $V_{C_c}$, and $V_o$ for steady-state operation can be described via (2), (4), (8), and (10) as

$$v_{C_s} = \frac{nV_i(2d-1)}{2(1-d)} \tag{20}$$

$$V_{C_c} = \frac{nV_i}{2(1-d)} \tag{21}$$

$$V_o = \frac{2+n}{2(1-d)}V_i \tag{22}$$

where $d$ is the duty cycle of the main switch ($S$). Continuously, the main switch ($S$) is turned ON at time $t = t_4$ to begin the next switching cycle.

Since the voltage difference may be caused by the secondary inductor of the transformer, as $d \neq 0.5$, the major function of the balanced capacitor ($C_c$) is used for keeping the cutoff voltages of the rectifier diodes ($D_1$, $D_2$, $D_3$, and $D_4$) balanced. Moreover, it also can avoid the overlarge current that passed through the rectifier diodes. According to (22), the voltage gain can be tuned by regulating the turns ratio ($n$) in the transformer to overcome the boost-ratio limitation of the conventional converter. In addition, the switch-voltage stress ($v_{DS}$) can be calculated via (11), (21), and (22) as

$$v_{DS} = \frac{V_i}{(1-d)}. \tag{23}$$

According to (22) and (23), one can obtain

$$v_{DS} = \frac{2V_o}{(2+n)}. \tag{24}$$

By analyzing (24), the switch-voltage stress ($v_{DS}$) is not related to the dc-input voltage ($V_i$) and duty cycle ($d$) if the values of the output voltage ($V_o$) and the turns ratio ($n$) are fixed. Thus, it can ensure that the sustainable voltage of the main switch ($S$) is constant. As long as the dc-input voltage is not higher than the rated voltage of the main switch, the high-efficiency voltage-clamped dc–dc converter can be applied well to the low-voltage power sources even with large voltage variations, e.g., fuel cell, solar cell, etc.

Fuel-cell generation systems have been receiving more attention in the last years due to the advantages of high-conversion efficiency, low aggression to the environment, no moving parts, and superior reliability and durability. Owing to the electrochemical reaction, fuel cell has the power quality of low voltage and high current. However, the fuel-cell stack with high output voltage is difficult to fabricate and it may be failure when any single cell is inactive. Besides, the output voltage is varied easily with respect to the load variations. In order to satisfy the requirement of high-voltage demand, a stable boost converter with high voltage gain and superior conversion efficiency is necessary to utilize the fuel-cell energy more efficiently. The validity of the proposed converter is verified by the following experimental results via an example of a PEMFC power source.

## III. Experimental Results

In order to verify the effectiveness of the designed converter topology, the clean energy of a PEMFC system is utilized for the low-voltage power source in the proposed high-efficiency voltage-clamped dc–dc converter, and its application circuit is depicted in Fig. 5. The PEMFC system used in this study is the PowerPEMTM-PS250 manufactured by the Hpower Company. It is a dc power source with 250-W dc nominal power rating. The system operates on an ambient air and clean pressurized-hydrogen fuel. The fuel-cell system consists of a (40) cell stack of the PEM type, mechanical auxiliaries, and electronic control module.

In experimentation, the high-efficiency voltage-clamped dc–dc converter is designed to operate from the fuel-cell variability dc input, $V_i = 27-37.5$ V, to deliver a constant dc output, $V_o = 200$ V, with the maximal capability of output power, $P_{o,max} = 330$ W. If the maximal value of main switch voltage ($v_{DS}$) is arranged for clamping at 50 V, the turns ratio can be determined as $n = (2V_o/v_{DS(max)}) - 2 = 6$ according to (24). As can be seen from Figs. 3 and 4, the voltage stress of the output diode ($v_{D_o}$) is the same as the switch-voltage stress. In addition, the voltage stresses of rectifier diodes ($v_{D_1}$, $v_{D_2}$, $v_{D_3}$, and $v_{D_4}$) can be calculated via (21) and (23) as $nv_{DS}/2 = 150$ V. For conservative consideration, the main switch (FQI90N08, 80 V), the output diode (Schottky diode SR20100, 100 V), and the rectifier diodes (Schottky diode SR20200, 200 V) are adopted in the experimental converter. In order to solve the problem of the fuel-cell output voltage varied with the variations of loads, the proposed converter with dc-voltage feedback control is utilized to ensure the system stability, and a PWM control IC TL494 is adopted to achieve this goal of feedback control. The prototype with the following specifications is designed in this section to illustrate the design procedure given in Section II:

| | |
|---|---|
| switching frequency | $f_s = 100$ kHz; |
| turns ratio | $n = 6$; |
| additional inductor | $L = 5.9$ $\mu$H; |
| primary inductor of transformer | $L_p = 213.6$ $\mu$H; |

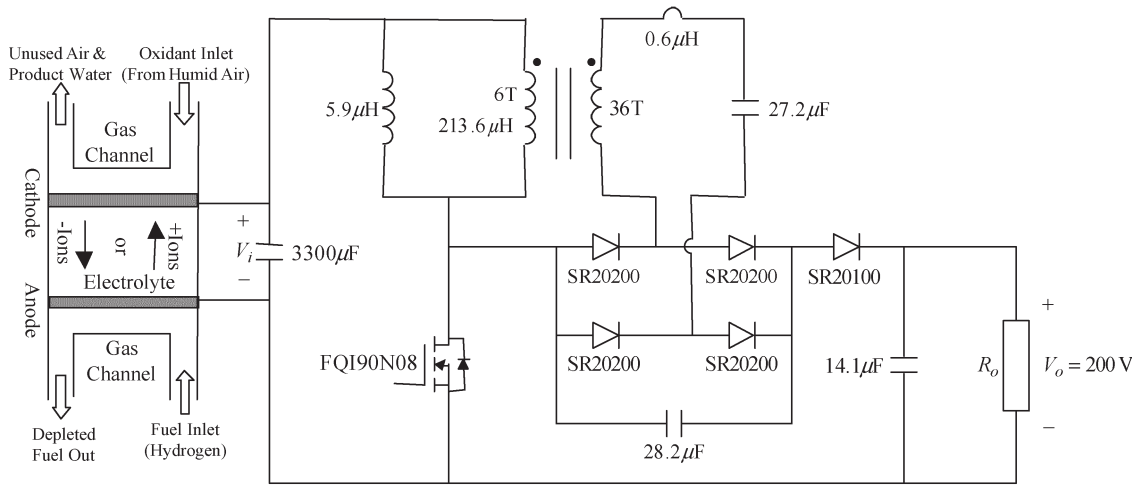


Fig. 5. Application circuit for the PEMFC system.

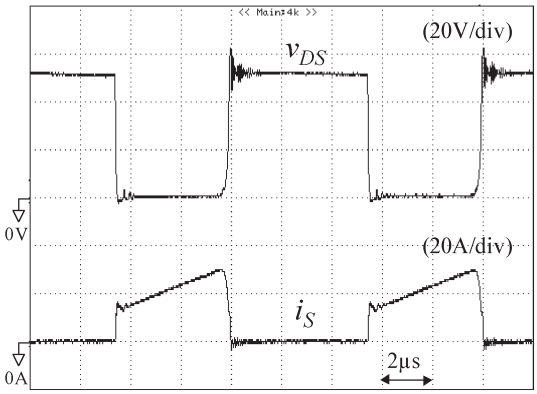


Fig. 6. Experimental voltage and current curves of main switch $S$ at 310-W output power.

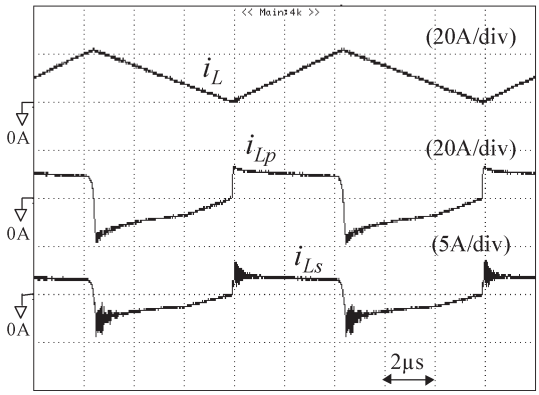


Fig. 7. Experimental current responses of additional inductor $L$, transformer primary inductor $L_{\rm p}$, and transformer secondary inductor $L_{\rm s}$ at 310-W output power.

secondary inductor of transformer $L_{\rm s} = 7689.6\ \mu$H;
secondary leakage inductor $L_{\rm k} = 0.6\ \mu$H;
balanced capacitor $C_{\rm s} = 4 \times 6.8\ \mu$F;
clamped capacitor $C_{\rm c} = 6 \times 4.7\ \mu$F;
input filter capacitor $C_{\rm i} = 3300\ \mu$F;
output filter capacitor $C_{\rm o} = 3 \times 4.7\ \mu$F;
main switch $S$: FQI90N08 (80 V, $R_{\rm DS(ON)} = 16\ {\rm m}\Omega$);
output diode $D_{\rm o}$: Schottky diode SR20100 (100 V, 20 A);
rectifier diodes $D_1$, $D_2$, $D_3$, $D_4$: Schottky diode SR20200 (200 V, 20 A).

Fig. 6 depicts the experimental voltage and current curves of the main switch $(S)$ at 310-W output power. As can be seen from this figure, the shaken switch voltage at the beginning is caused by the line inductor when the switch is turned OFF. Fortunately, the steady state of this switch-voltage stress is about 50 V due to the utilization of voltage-clamped technique, and it is much smaller than the output voltage, $V_{\rm o} = 200$ V. It has the merit of selecting a low-voltage-rated device in order to reduce the conduction loss of the switch. The experimental current waveforms of the additional inductor $(L)$, in parallel with the transformer, primary inductor of transformer $(L_{\rm p})$, and secondary inductor of transformer $(L_{\rm s})$ at 310-W output power, are depicted in Fig. 7. By observing the currents of $i_{L_{\rm p}}$ and $i_{L_{\rm s}}$, it is obvious that the transformer is manipulated during the four-quadrant operation so that the utility rate of the magnetic core is improved to exhibit the transformer characteristics completely. The experimental voltage and current responses of the diodes ($D_{\rm o}$, $D_3$, and $D_4$) at 310-W output power are depicted in Fig. 8. From these results, the reverse-recovery currents in these diodes are small to give the credit to the utilization of Schottky diodes with extremely low switching and conduction losses. Thus, it can alleviate the reverse-recovery problem for further raising the conversion efficiency. As can been seen from Fig. 8(b) and (c), the balanced capacitor $(C_{\rm s})$ can be used for balancing the current and cutoff voltage of the diodes ($D_3$ and $D_4$) when the condition of $d \neq 0.5$ holds.

For verifying the voltage-clamped property, the experimental voltage responses of the output voltage $(V_{\rm o})$, clamped capacitor $(C_{\rm c})$, output diode $(D_{\rm o})$, and main switch $(S)$ at 310-W output power are depicted in Fig. 9. As can be seen from this figure, the output voltage, $V_{\rm o} = 200$ V, is strode mainly across the clamped capacitor in the secondary-side circuit (i.e., $V_{C_{\rm c}} = 150$ V). Thus, the switch-voltage stress and the cutoff voltage

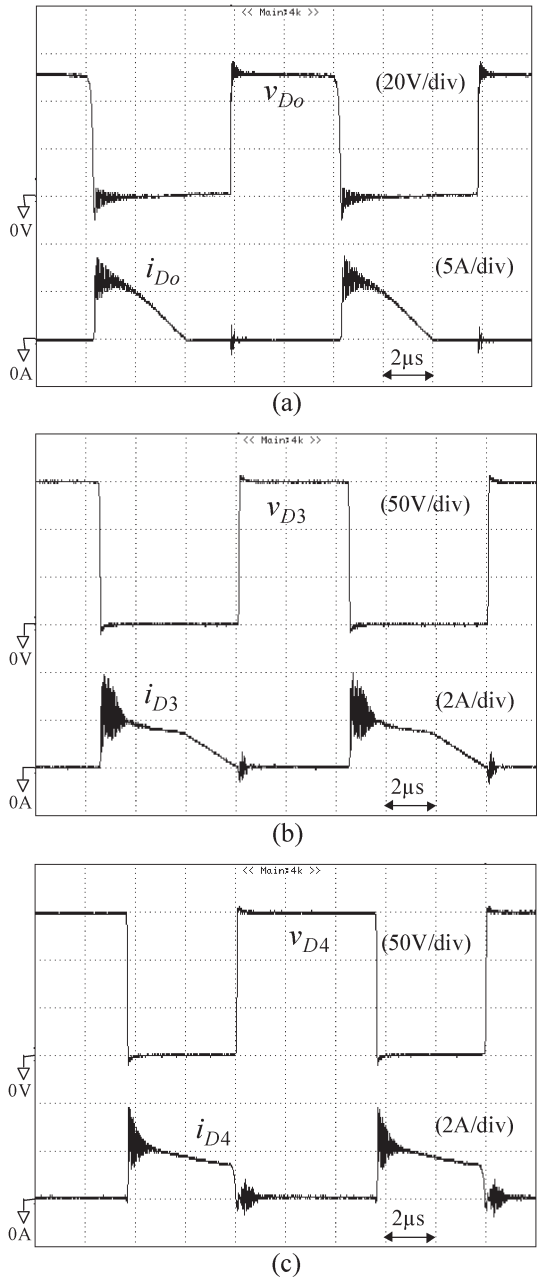


Fig. 8. Experimental voltage and current responses of diodes at 310-W output power. (a) $D_o$. (b) $D_3$. (c) $D_4$.

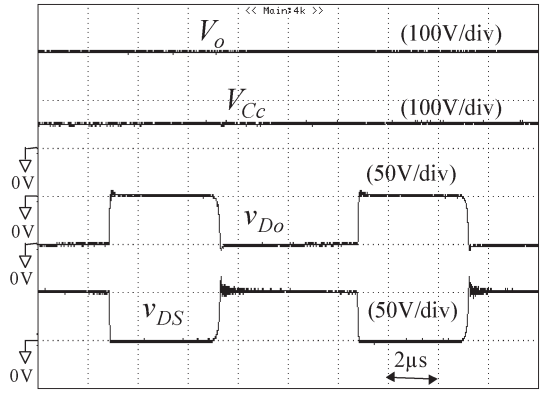


Fig. 9. Experimental voltage responses of output voltage $V_{\rm o}$, clamped capacitor $C_{\rm c}$, output diode $D_{\rm o}$, and main switch $S$ at 310-W output power.

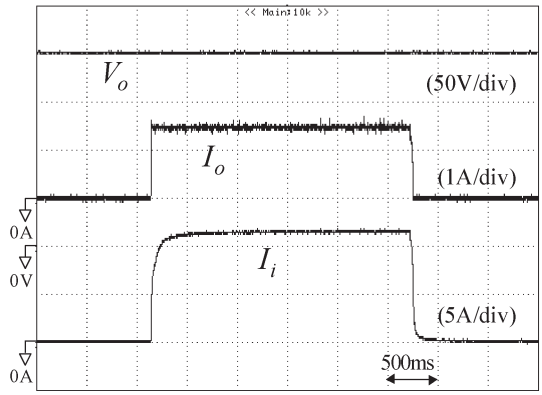


Fig. 10. Experimental results of converter output voltage $V_{\rm o}$, output current $I_{\rm o}$, and PEMFC output current $I_{\rm i}$ under step load variation between no load (0 W) and full load (310 W).

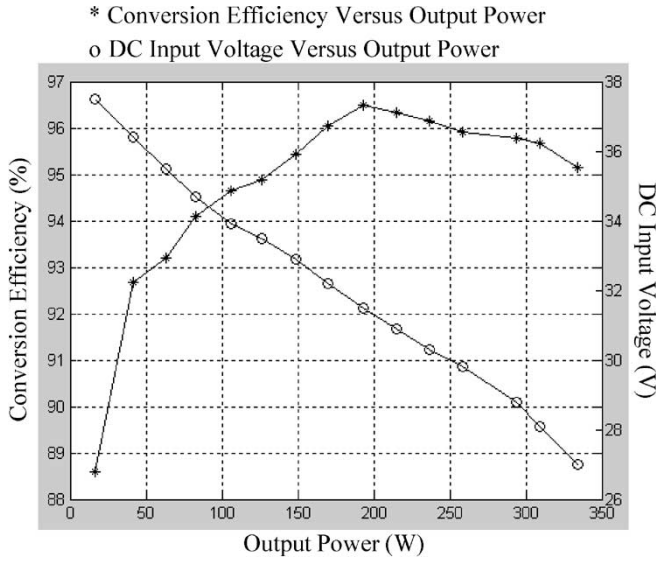


Fig. 11. Converter efficiency and PEMFC output voltage under different output powers.

of the output diode are clamped at about 50 V. In order to examine the robust performance of the proposed converter scheme, the experimental results of the converter output voltage $(V_{\rm o})$, output current $(I_{\rm o})$, and the PEMFC output current $(I_{\rm i})$ under the step load variation between no load (0 W) and full load (310 W) are depicted Fig. 10. According to Fig. 10, the converter output voltage, $V_{\rm o} = 200$ V, is insensitive to the variation of loads due to the closed-loop control, and the output current ripple is also slightly extreme as a result of the high switching frequency. Fig. 11 summarizes the conversion efficiency of the proposed converter and the PEMFC output voltage under different output powers. From the experimental results, the measure of efficiency of the proposed converter operating at 310-W output power is 95.6%, and the maximal efficiency is 96.5% at 190-W output power. The above experimental results agree well with those obtained from the design procedure given in Section II. However, slight differences in these results are attributed to the factor of system uncertainties in practical applications.

## IV. Conclusion

This paper has successfully developed a high-efficiency voltage-clamped dc–dc converter with reduced reverse-recovery current and switch-voltage stress, and this converter has been applied well to a PEMFC system with a power quality of low voltage and high current. According to the experimental results, the maximal efficiency was measured to be over 96%, which is comparatively higher than the conventional converter with the same voltage gain. The newly designed converter circuit has the following improvements compared to the previous work.

1) It can select the main switch with lower sustainable voltage for alleviating the switch conduction loss due to the utilization of voltage-clamped technique.
2) All diodes in this circuit topology are Schottky diodes with the reduction of switching and conduction losses.
3) The additional inductor is used for providing the reverse-current path of the transformer to raise the utility rate of the magnetic core.
4) Additional snubber circuits for absorbing the voltage spikes in the diodes are not required to further cut down the manufacture cost.
5) There is no circulating current to overcome the problem of degenerate efficiency under slight loads.
6) The voltage-drift problem of power source under the variation of loads can be solved by the closed-loop control methodology.

This new converter topology provides designers with an alternative choice to convert renewable energy efficiently, and it also can be extended easily to other power-conversion systems for satisfying high-voltage demands.

## Acknowledgment

The authors would like to express their gratitude to the Referees and the Associate Editor for their useful comments and suggestions.

## References

[1] I. Barbi and R. Gules, "Isolated dc–dc converters with high-output voltage for TWTA telecommunication satellite applications," *IEEE Trans. Power Electron.*, vol. 18, no. 4, pp. 975–984, Jul. 2003.
[2] O. Abutbul, A. Gherlitz, Y. Berkovich, and A. Ioinovici, "Step-up switching-mode converter with high voltage gain using a switched-capacitor circuit," *IEEE Trans. Circuits Syst. I, Fundam. Theory Appl.*, vol. 50, no. 8, pp. 1098–1102, Aug. 2003.
[3] K. C. Tseng and T. J. Liang, "Novel high-efficiency step-up converter," *Proc. Inst. Elect. Eng.—Electr. Power Appl.*, vol. 151, no. 2, pp. 182–190, Mar. 2004.
[4] N. Mohan, T. M. Undeland, and W. P. Robbins, *Power Electronics: Converters, Applications, and Design*. New York: Wiley, 1995.
[5] M. M. Jovanovic and Y. Jang, "A new soft-switched boost converter with isolated active snubber," *IEEE Trans. Ind. Appl.*, vol. 35, no. 2, pp. 496–502, Mar./Apr. 1999.
[6] C. M. C. Duarte and I. Barbi, "An improved family of ZVS-PWM active-clamping DC-to-DC converters," *IEEE Trans. Power Electron.*, vol. 17, no. 1, pp. 1–7, Jan. 2002.
[7] E. S. da Silva, L. dos Reis Barbosa, J. B. Vieira, L. C. de Freitas, and V. J. Farias, "An improved boost PWM soft-single-switched converter with low voltage and current stresses," *IEEE Trans. Ind. Electron.*, vol. 48, no. 6, pp. 1174–1179, Dec. 2001.
[8] K. Hirachi, M. Yamanaka, K. Kajiyama, and S. Isokane, "Circuit configuration of bidirectional DC/DC converter specific for small scale load leveling system," in *Proc. IEE Power Conversion Conf.*, Osaka, Japan, 2002, pp. 603–609.
[9] C. W. Roh, S. H. Han, and M. J. Youn, "Dual coupled inductor fed isolated boost converter for low input voltage applications," *Electron. Lett.*, vol. 35, no. 21, pp. 1791–1792, Oct. 1999.
[10] Q. Zhao and F. C. Lee, "High-efficiency, high step-up dc–dc converters," *IEEE Trans. Power Electron.*, vol. 18, no. 1, pp. 65–73, Jan. 2003.
[11] K. Ro and S. Rahman, "Two-loop controller for maximizing performance of a grid-connected photovoltaic-fuel cell hybrid power plant," *IEEE Trans. Energy Convers.*, vol. 13, no. 3, pp. 276–281, Sep. 1998.
[12] M. D. Lukas, K. Y. Lee, and H. Ghezel-Ayagh, "Development of a stack simulation model for control study on direct reforming molten carbonate fuel cell power plant," *IEEE Trans. Energy Convers.*, vol. 14, no. 4, pp. 1651–1657, Dec. 1999.
[13] ——, "An explicit dynamic model for direct reforming carbonate fuel cell stack," *IEEE Trans. Energy Convers.*, vol. 16, no. 3, pp. 289–295, Sep. 2001.
[14] A. Boudghene Stambouli and E. Traversa, "Fuel cells, an alternative to standard sources of energy," *Renew. Sustain. Energy Rev.*, vol. 6, no. 3, pp. 297–306, Sep. 2002.
[15] M. W. Ellis, M. R. Von Spakovsky, and D. J. Nelson, "Fuel cell systems: Efficient, flexible energy conversion for the 21st century," *Proc. IEEE*, vol. 89, no. 12, pp. 1808–1818, Dec. 2001.
[16] J. M. Correa, F. A. Farret, J. R. Gomes, and M. G. Simoes, "Simulation of fuel-cell stacks using a computer-controlled power rectifier with the purposes of actual high-power injection applications," *IEEE Trans. Ind. Appl.*, vol. 39, no. 4, pp. 1136–1142, Jul./Aug. 2003.
[17] K. Green and J. C. Wilson, "Future power sources for mobile communications," *IEE Electron. Commun. Eng. J.*, vol. 13, no. 1, pp. 43–47, Feb. 2001.

**Rong-Jong Wai** (M'99–A'00–M'02–SM'05) was born in Tainan, Taiwan, R.O.C., in 1974. He received the B.S. degree in electrical engineering and the Ph.D. degree in electronic engineering from Chung Yuan Christian University, Chung Li, Taiwan, R.O.C., in 1996 and 1999, respectively.

Since 1999, he has been with the Department of Electrical Engineering, Yuan Ze University, Chung Li, Taiwan, R.O.C., where he is currently a Professor. He is also the Director of the Electric Control and System Engineering Laboratory at Yuan Ze University, Chung Li, Taiwan, R.O.C. and the Energy Conversion and Power Conditioning Laboratory at the Fuel Cell Center. He is the Chapter Author of *Intelligent Adaptive Control: Industrial Applications in the Applied Computational Intelligence Set* (CRC Press, 1998) and the coauthor of *Drive and Intelligent Control of Ultrasonic Motor* (Tsang-Hai, 1999), *Electric Control* (Tsang-Hai, 2002), and *Fuel Cell: New Generation Energy* (Tsang-Hai, 2004). He has authored numerous published journal papers in the area of control system applications. His research interests include power electronics, motor servo drives, mechatronics, energy technology, and control theory applications.

Dr. Wai received the Excellent Research Award in 2000, and the Wu Ta-You Medal and Young Researcher Award in 2003 from the National Science Council, R.O.C. In addition, he was the recipient of the Outstanding Research Award in 2003 from the Yuan Ze University, R.O.C.; the Excellent Young Electrical Engineering Award in 2004 from the Chinese Electrical Engineering Society, R.O.C; the Outstanding Professor Award in 2004 from the Far Eastern Y. Z. Hsu-Science and Technology Memorial Foundation, R.O.C.; the International Professional of the Year Award in 2005 from the International Biographical Centre; and the Young Automatic Control Engineering Award in 2005 from the Chinese Automatic Control Society, R.O.C. His biography was listed in *Who's Who in Science and Engineering* (Marquis Who's Who) in 2003, *Who's Who* (Marquis Who's Who) in 2005, and *Leading Scientists of the World* (International Biographical Centre) in 2005.

**Li-Wei Liu** was born in Chang-hua, Taiwan, R.O.C., in 1980. He received the B.S. and M.S. degrees in electrical engineering from Yuan Ze University, Chung Li, Taiwan, R.O.C., in 2003 and 2005, respectively.

He is currently an R&D Engineer in the Department of Test and Measurement, Chroma Company, Taipei, Taiwan, R.O.C. His research interests include motor servo drives, power electronics, and renewable energy.

**Rou-Yong Duan** was born in Nantou, Taiwan, R.O.C., in 1965. He received the B.S. degree from National Kaohsiung University of Applied Sciences, Kaohsiung, Taiwan, R.O.C., in 1986, the M.S. degree from Chung Yuan Christian University, Chung Li, Taiwan, R.O.C., in 1998, and the Ph.D. degree from Yuan Ze University, Chung Li, Taiwan, R.O.C., in 2004, all in electrical engineering.

Since August 2004, he has been an Assistant Professor at the Department of Industrial Safety and Health, Hung Kuang University, Tai Chung, Taiwan, R.O.C. His research interests include motor servo drives, resonant theory, power electronics, and renewable energy.